SIMULATION OF CRITICAL HEAT FLUX EXPERIMENTS IN NEPTUNE_CFD CODE

J. Macek, L. Vyskocil

Nuclear Research Institute Rez (NRI), Dept. of Thermal Hydraulic Analyses,
250 68 Rez, Czech Republic

Abstract

This paper presents a CFD simulation of selected "Large Water Loop" critical heat flux experiments. Calculations were performed by NEPTUNE_CFD code. The Large Water Loop (LWL) is non-active pressurised-water equipment with technological and thermal parameters corresponding to those of PWR. The CHF experimental facility (a part of the Large Water Loop) has been designed for research into CHF in water flow through a bundle of electrically heated vertical rods. The critical conditions were determined under constant pressure, inlet water temperature and mass flux and for quasi steady-state - by gradually increasing the heat input. The rods are modelled by hollow tubes with direct heating of the wall.

Thirteen CHF tests were calculated with NEPTUNE. In all calculated tests, a sudden rise of the wall temperature was observed. Simulations of cases with a higher mass flux were successful. Simulation of cases with a low mass flux indicates that the modelling approach might not be suitable for lower mass fluxes.

The results show that NEPTUNE has some potential for predicting boiling flow up to CHF in the geometry of reactor fuel assembly.

The presented work was carried out as part of the NURESIM project. NEPTUNE_CFD code is implemented in the NURESIM platform.

1. INTRODUCTION

The application of boiling is limited by a condition called critical heat flux (CHF). The most serious problem is that the boiling limitation can be directly related to the physical burnout of the materials of a heated surface due to the suddenly inefficient heat transfer through a vapour film formed across the surface resulting from the replacement of liquid by vapour adjacent to the heated surface.

In a surface-heat-flux-controlled system, the occurrence of CHF is accompanied by an inordinate increase in the surface temperature. Otherwise, an excessive decrease of the heat transfer rate occurs for a surface-temperature-controlled system.

2. THE LARGE WATER LOOP EXPERIMENTAL FACILITY

The Large Water Loop (LWL) has been built at the Nuclear Machinery Plant, Skoda, Plzen Ltd., Czech Republic (see Bestion et al. 2006). The loop is non-active pressurised-water equipment with technological and thermal parameters corresponding to those of PWR. The possible parameters ranges are suitable for all types of pressurised water reactors.

The CHF experimental facility (a part of the Large Water Loop) has been designed for research into CHF in water flow through a bundle of electrically heated vertical rods (nineteen 9.1mm diameter and 12.75mm pitch rods). The heated length is 3.5m. The critical conditions were determined under constant pressure, inlet water temperature and mass flux and for a quasi steady-state by gradually increasing the heat input.

The rods are modelled using hollow tubes with direct heating of the wall. The axial distribution of the wall heat flux is uniform while the radial distribution varies from power coefficient of 1 for the central rod to 0.75 for the outer rods (see Fig. 1).
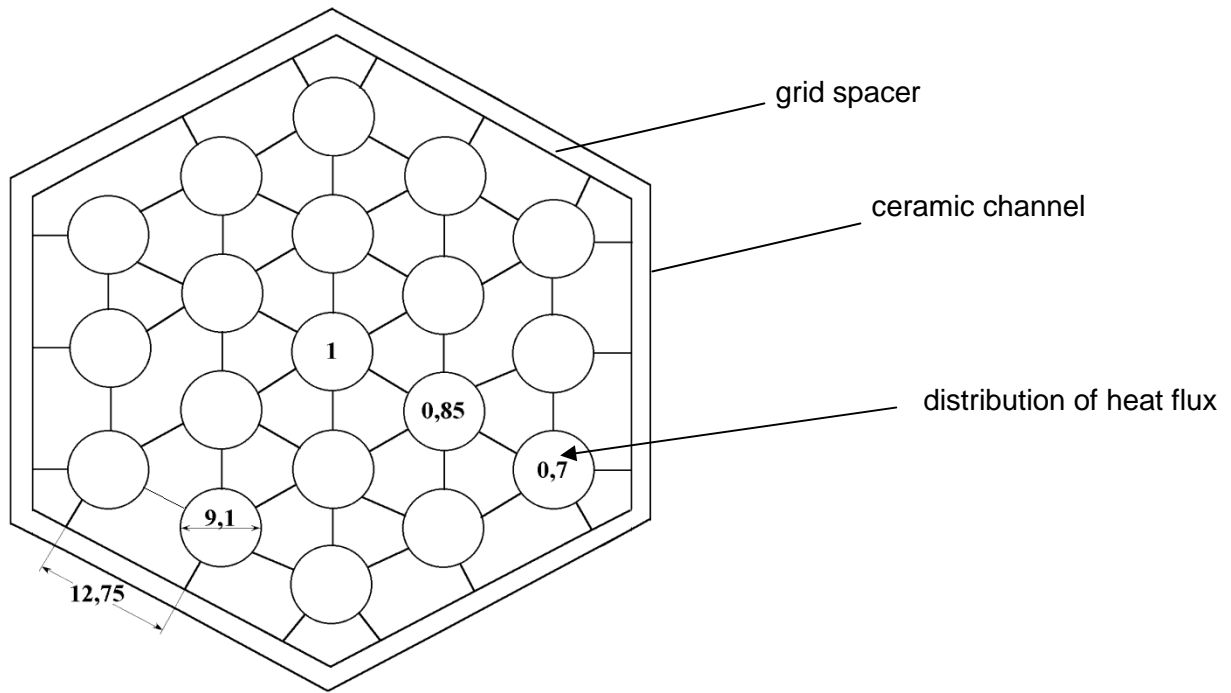
Fig. 1   LWL – Bundle D: horizontal cross section, power coefficients

3. SELECTED TEST CASES

The following table shows the experimental data set used in NEPTUNE simulations:

	p_{in}	T_{in}	T_{sat}	mf	q_{CHF}
	[MPa]	[°C]	[°C]	[kg/s/m^2]	[W/m^2]
Case 1	14.407	292.13	338.94	1236	725080
Case 2	14.136	284.88	337.43	1350	781922
Case 3	10.679	243.59	315.86	569	716068
Case 4	12.627	308.67	328.59	1225	625260
Case 5	11.938	249.94	324.28	2062	1180507
Case 6	9.952	242.2	310.64	1531	1057812
Case 7	10.367	237.45	313.66	2458	1403022
Case 8	10.179	269.31	312.30	2937	1217940
Case 9	16.058	151.22	347.65	979	1070983
Case 10	16.254	266.03	348.63	996	674477
Case 11	12.466	230.95	327.60	503	648135
Case 12	14.1	300.41	337.23	4795	1646333
Case 13	17.846	300.41	356.28	3837	1575627

Table 1: Selected LWL Test Cases

p_{in} and T_{in} are the inlet pressure and temperature. T_{sat} is the saturation temperature, mf is the mass flux, q_{CHF} is the critical heat flux on the central rod.

4. MODELING OF BOILING FLOW UNDER CHF CONDITIONS

This chapter describes the generalized boiling model, which is implemented in NEPTUNE code and used for simulating LWL experiments. The presented model simulates the onset of nucleate boiling, partitioning of the wall heat flux and interfacial liquid-vapour heat, momentum and mass transfer.

Two phases are modelled: the primary phase is liquid and the secondary is vapour bubbles. The same pressure is shared by the two phases. Continuity, momentum and energy equations are solved for each phase. The "k-ε liq" model (Yao, Morel 2004) is used for modelling the liquid turbulence; the flow of vapour is assumed to be laminar. Distribution of the mean bubble diameter in the flow is modelled using a one-group interfacial area transport equation.

4.1 Onset of Nucleate Boiling

When the wall becomes superheated, vapour bubbles can form even when the core liquid is still subcooled. The position where the first bubbles occur at the wall is denoted as the onset of nucleate boiling. In our calculations, Hsu's criterion is used to determine this position (Hsu, 1962). According to this criterion, a bubble will grow from a vapour embryo occupying a cavity in the wall if the liquid temperature at the tip of the embryo is at least equal to the saturation temperature corresponding to the bubble pressure.

4.2 Basic Wall Heat Flux Partitioning Model

The heat flux partitioning model of Kurul and Podowski (1990) (see also Yao, Morel 2002, 2004) has the following structure:
Downstream of the onset of nucleate boiling, the wall heat flux q_{wall} is split into three parts:

$$q_{wall} = q_f + q_q + q_e \quad \left[W/m^2\right] \tag{1}$$

The first part is the single-phase heat transfer (convective heat flux):

$$q_f = A_1 \alpha_{wallfcn} \left(T_{wall} - T_l\right) \tag{2}$$

$$A_1 = 1 - A_2 \tag{3}$$

A_1 is the fraction of the wall surface influenced by the liquid, fraction A_2 is influenced by vapour bubbles formed on the wall, T_l is the liquid temperature at the centre of the wall adjacent cell, $\alpha_{wallfcn}$ is the wall heat transfer coefficient calculated from the temperature wall function.

The quenching part q_q of the heat flux q_{wall} is transported by transient conduction during the time period between the bubble departure and the next bubble formation at the same nucleation site.

$$q_q = A_2 \alpha_{quench} \left(T_{wall} - T_l\right) \tag{4}$$

α_{quench} is the quenching heat transfer coefficient (17).
Heat flux q_e is spent for liquid evaporation:

$$q_e = \dot{m}_e H_{lat} \tag{5}$$

$\dot{m}_e$ is the evaporation mass transfer per the unit wall area (15), H_{lat} is the latent heat.

The model assumes that the diameter of the area influenced by a single bubble is as large as the bubble departure diameter d_w:

$$A_2 = \min\left(\frac{\pi \cdot d_w^2 \cdot n}{4}, 1\right) \tag{6}$$

n is the active nucleation site density.

The active nucleation site density is correlated to the wall superheat:

$$n = \left(210 \cdot \left(T_{wall} - T_{sat}\right)\right)^{1.8} \quad \left[\frac{1}{m^2}\right] \tag{7}$$

The bubble departure diameter d_w is calculated from Ünal correlation (Ünal, 1976):

$$d_w = 2.42 \cdot 10^{-5} \, p^{0.709} \frac{a}{\sqrt{b\phi}} \quad [m] \tag{8}$$

where p is pressure [Pa],

$$a = \frac{(T_w - T_{sat})\lambda_s}{2\rho_v H_{lat} \sqrt{\pi a_s}} \tag{9}$$

a_s is the thermal diffusivity and λ_s is the thermal conductivity of the solid wall

$$b = \frac{T_{sat} - T_l}{2(1 - \rho_v / \rho_l)} \quad for\ St < 0.0065 \tag{10}$$

$$b = \frac{q_{wall}}{2(1 - \rho_v / \rho_l) \cdot 0.0065 \cdot \rho_l c_{pl} U_l} \quad for\ St \geq 0.0065 \tag{11}$$

where:

$$St = \frac{q_{wall}}{\rho_l c_{pl} U_l (T_{sat} - T_l)} \quad \text{(Stanton number)} \tag{12}$$

U_l is the liquid velocity magnitude at the wall adjacent cell

$$\phi = \max\left(1, \left(\frac{U_l}{0.61}\right)^{0.47}\right) \tag{13}$$

When $T_l > T_{sat}$, bulk boiling is initiated.

To calculate the evaporation rate $\dot{m}_e$, the bubble detachment frequency f is determined from the following equation:

$$f = \sqrt{\frac{4 \cdot g \cdot (\rho_l - \rho_v)}{3 \cdot d_w \cdot \rho_l}} \quad \left[\frac{1}{s}\right] \tag{14}$$

The evaporation rate is the product of bubble mass, detachment frequency and the active nucleation site density:

$$m_e = \frac{\pi \cdot d_w^{\,3}}{6} \rho_v \cdot f \cdot n \quad \left[\frac{kg}{m^2 s}\right] \tag{15}$$

The quenching heat transfer coefficient α_{quench} depends on the waiting time between bubble departure and the next bubble formation. This waiting time t_w is fixed to the bubble detachment period:

$$t_w = \frac{1}{f} \quad [s] \tag{16}$$

$$\alpha_{quench} = 2 \cdot \lambda_l \cdot f \cdot \sqrt{\frac{t_w}{\pi \cdot a_l}} \quad \left[\frac{W}{m^2 K}\right] \tag{17}$$

where a_l is the liquid thermal diffusivity.

4.3 Generalization of the Wall Heat Flux Partitioning Model

The basic wall heat flux partitioning model presented in chapter 4.2 assumes that the amount of water on the wall is sufficient to remove heat from the wall and to be used for evaporation. Superheating of the vapour that occurs at high void fractions is not modelled. Given all this, the basic heat flux partitioning model cannot be used under critical heat flux conditions.

In order to account for a critical heat flux condition, the heat flux partitioning model can be generalized as follows:

$$q_{wall} = f_{\alpha 1}(q_f + q_q + q_e) + (1 - f_{\alpha 1})q_v \quad [W / m^2] \tag{18}$$

The fourth part of the wall heat flux, q_v, is the diffusive heat flux given to the vapour phase:

$$q_v = \alpha_{wallfcn,v}\left(T_{wall} - T_v\right) \tag{19}$$

$\alpha_{wallfcn,v}$ is the wall heat transfer coefficient calculated from the temperature wall function for the vapour phase, T_v is the vapour temperature at the centre of the wall-adjacent cell.

$f_{\alpha 1}$ is the phenomenological function, which depends on the liquid volume fraction α_1. $f_{\alpha 1}$ must fulfil the following conditions:

$$f_{\alpha 1} \to 1 \quad if \quad \alpha_1 \to 1, \quad f_{\alpha 1} \to 0 \quad if \quad \alpha_1 \to 0 \tag{20}$$

$$\frac{f_{\alpha 1}}{\alpha_1} \to 0 \quad if \quad \alpha_1 \to 0, \quad \frac{1 - f_{\alpha 1}}{1 - \alpha_1} \to 0 \quad if \quad \alpha_1 \to 1 \tag{21}$$

The "EDF wall-fluid heat transfer" model (see Lavieville et al. 2005) that is implemented in NEPTUNE and used in our calculations assumes function $f_{\alpha 1}$ in the following form:

$$\alpha_1 > \alpha_{1,crit} : \quad f_{\alpha 1} = 1 - \frac{1}{2}\exp\left[-20\left(\alpha_1 - \alpha_{1,crit}\right)\right] \tag{22}$$

$$\alpha_1 < \alpha_{1,crit} : \quad f_{\alpha 1} = \frac{1}{2}\left(\frac{\alpha_1}{\alpha_{1,crit}}\right)^{20\alpha_{1,crit}} \tag{23}$$

$$\alpha_{1,crit} = 0.2$$

i.e. the critical value for the void fraction is $1 - \alpha_{1,crit} = 0.8$. Note that Weisman DNB criterion is void fraction=0.82 (Weisman 1983).

4.4 Interfacial Momentum Transfer

The interfacial momentum transfer can be divided into four parts: drag, virtual mass force, lift and turbulent dispersion (Lance, Lopez de Bertodano, 1994, Yao, Morel 2002, 2004).

The interfacial drag force is calculated as:

$$\vec{M}_v^D = -\vec{M}_l^D = 0.75\frac{\alpha_v}{d_b}\rho_l c_D\left|\vec{V}_l - \vec{V}_v\right|\left(\vec{V}_l - \vec{V}_v\right) \tag{24}$$

d_b is the Sauter mean bubble diameter calculated from the interfacial area transport equation, the drag coefficient c_D is calculated by Inclusions (EDF) model (Lavieville et al. 2005).

The lift force was not included in our calculations because it caused convergence problems.

The added mass force is given by: (Zuber, 1964)

$$\vec{M}_v^{AM} = -\vec{M}_l^{AM} = c_{AM}\frac{1 + 2\alpha_v}{1 - \alpha_v}\alpha_v\rho_l\left[\left(\frac{\partial \vec{V}_l}{\partial t} + \vec{V}_l \cdot \nabla \vec{V}_l\right) - \left(\frac{\partial \vec{V}_v}{\partial t} + \vec{V}_v \cdot \nabla \vec{V}_v\right)\right] \tag{25}$$

The added mass force coefficient is $c_{AM} = 0.5$.

The turbulent dispersion force is given by:

$$M_v^{TD} = -M_l^{TD} = -c_{TD} \cdot \rho_l \cdot k_l \cdot \nabla \alpha_v \tag{26}$$

The turbulent dispersion coefficient is set to $c_{TD} = 2.5$ (Yao, Morel 2002, 2004). k_l is the turbulence kinetic energy of the liquid.

4.5 Interfacial Heat Transfer

Interface to liquid heat transfer – "ASTRID-like model" (Lavieville et al. 2005):

$$Q_{li} = \frac{6\alpha_v Nu\lambda_l}{d_b^{\ 2}}\left(T_{sat} - T_l\right) \quad \left[W/m^3\right] \tag{27}$$

d_b is the Sauter mean bubble diameter, λ_l is the liquid thermal conductivity.

The Nusselt number Nu is calculated from:

$$Nu = 2 + 0.6\,\text{Re}^{0.5}\,\text{Pr}^{0.33} \tag{28}$$

$$\text{Re} = \frac{\rho_l d_b \cdot V_{rel}}{\mu_l} \tag{29}$$

$$\text{Pr} = \frac{\mu_l \cdot c_{p,l}}{\lambda_l} \tag{30}$$

Re is the Reynolds number, Pr is the Prandtl number of the liquid, V_{rel} is the magnitude of relative velocity between phases, μ_l is the dynamic viscosity of the liquid, $c_{p,l}$ is the liquid heat capacity.

Interface to vapour heat transfer:
The interface to vapour heat transfer is calculated with help of the "constant time scale return to saturation" method (Lavieville et al. 2005b).

$$Q_{vi} = \frac{\alpha_v \rho_v c_{P,v}}{\Delta t}\left(T_{sat} - T_v\right) \quad \left[\frac{W}{m^3}\right] \tag{31}$$

$\Delta t = 0.05s$ is the time scale, $c_{P,v}$ is the isobaric heat capacity of the vapour.
The interfacial mass transfer depends directly on the interfacial heat transfer.

4.6 Interfacial Area Transport

The Sauter mean bubble diameter distribution in the flow was calculated from the interfacial area concentration. The one group equation of the interfacial area concentration transport with models for coalescence and break-up (Yao and Morel 2004; Morel, Yao, Bestion, 2003) is used to describe the evolution of the interfacial area concentration.

5. CALCULATION OF LWL EXPERIMENTS IN NEPTUNE

5.1 Computational Grid

The computational domain covers a 30° symmetric section of the actual channel. Grid spacers are not modelled.
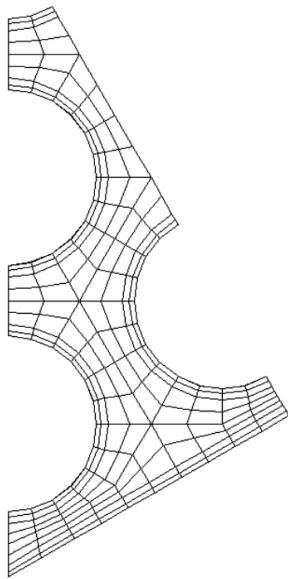The cutting planes are modelled as a symmetry boundary condition.

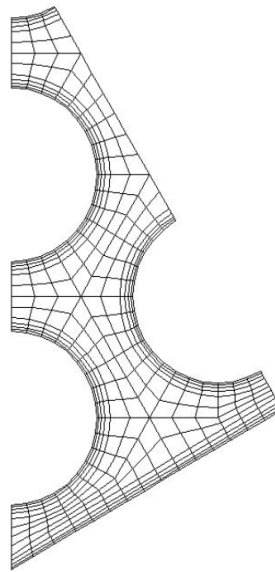**Fig. 2   Coarse Grid**   **Fig. 3   Fine Grid**

Two computational grids were created - see Fig. 2 and Fig. 3. The coarse grid consists of 76,800 hexahedral cells. In the vertical direction (3.5m height), there are 400 intervals. The fine grid is subdivided into 150,000 hexahedral cells. Resolution in the vertical direction is the same as in the case of the coarse grid. The fine grid was used successfully for the preliminary single-phase calculation. When it was used to simulate actual LWL experiments, the calculations ended up with very small time steps and it was impossible to finish the calculation in a reasonable time. With the coarse grid there were no such problems. It was therefore decided to use the coarse grid for all calculations.

5.2 NEPTUNE Settings

- Turbulence modelling: "k-epsilon liq" model for the liquid, laminar flow of vapour
- Turbulent reverse coupling – influence of phase 2 on phase 1
- Turbulent dispersion force based on the void fraction gradient, turbulent dispersion coefficient c_{TD} was set to 2.5 – used from Yao, Morel (2002)
- Drag force: inclusions(EDF) model (Lavieville, 2005b), Ishii (1979) model caused calculation "freezing" (very low time steps) when bubbles entered distorted regime
- Added mass force by Zuber, no lift force (lift force caused instabilities)
- Wall-fluid heat transfer: EDF wall-fluid heat transfer (generalized heat flux decomposition, super-heated vapour empirical model based on a local void fraction critical value of 0.8, see chapter 4.3)
- Interface heat transfer: Astrid-like model for liquid, relaxation time for vapour
- CATHARE tables – Water std. rev6 extended
- The mean bubble diameter is calculated from the interfacial area
- Interfacial area transport: one group approach (one mean bubble diameter in each individual cell), coalescence and break-up of bubbles: Yao's models (2004)

NEPTUNE version: 1.0.5

5.3 Calculation Procedure

The actual experiments are quasi-steady. The inlet temperature, pressure and mass flux are constant and wall heat fluxes are gradually increasing. The maximum temperature gradient is 2°C/min so the transients are too long to be calculated by NEPTUNE in a reasonable time. We decided to calculate the flow with steady boundary conditions (i.e. constant wall heat fluxes).

In some cases, it was impossible to perform the calculation with 100% wall heat fluxes from the beginning because there were convergence troubles directly after the start-up when large amounts of vapour were created on the walls and then condensed. The procedure that worked for all cases was to calculate the first 0.1s with 10% wall heat fluxes, then raise the heat fluxes to 50% and let the flow stabilize. This took 2-5seconds of transient (depending on the mass flux). Then the wall heat fluxes were increased to 100%. Again, we let the flow stabilize. When the flow rate (liquid + vapour) leaving the domain was equal to the inlet flow rate and the wall temperatures and other parameters were stabilized, we analyzed the results. Depending on the results, wall heat fluxes were decreased or increased so as to find out the interval of the wall heat fluxes where a sudden increase of wall temperature occurs.

6. RESULTS

The calculation results are shown in the following table:

	p_{in}	T_{in}	T_{sat}	mf	q_{CHF}	q_{calc}/q_{CHF}	α_{max}	$(T_w-T_{sat})_{max}$	CHF
	[MPa]	[°C]	[°C]	[kg/s/m^2]	[W/m^2]		[m^3/m^3]	[K]	
Case 1	14.407	292.13	338.94	1236	725080	100%	0.847	19.6	+
						90%	0.788	13.5	+ -
Case 2	14.136	284.88	337.43	1350	781922	100%	0.836	19	+
						90%	0.77	14	-
Case 3	10.679	243.59	315.86	569	716068	75%	0.914	650	+
						60%	0.825	14.3	+
						50%	0.699	11.7	-
Case 4	12.627	308.67	328.59	1225	625260	100%	0.895	304	+
						90%	0.861	19.2	+
						80%	0.816	13.1	+ -
Case 5	11.938	249.94	324.28	2062	1180507	100%	0.835	26.1	+
						90%	0.748	17	-
Case 6	9.952	242.2	310.64	1531	1057812	90%	0.888	551.3	+
						80%	0.829	19.92	+
						70%	0.737	15.2	-
Case 7	10.367	237.45	313.66	2458	1403022	100%	0.877	619	+
						90%	0.806	20.7	+ -
						80%	0.681	17.4	-
Case 8	10.179	269.31	312.30	2937	1217940	100%	0.863	193.1	+
						90%	0.804	17.8	+ -
Case 9	16.058	151.22	347.65	979	1070983	100%	0.6003	17.7	-
						110%	0.805	20.54	+
Case 10	16.254	266.03	348.63	996	674477	100%	0.71	13.67	-
						110%	0.803	15.05	+ -
Case 11	12.466	230.95	327.60	503	648135	90%	0.9204	783.78	+
						80%	0.8769	38.57	+
						75%	0.8405	17.09	+
						60%	0.6552	12.02	-
Case 12	14.1	300.41	337.23	4795	1646333	100%	0.98*	2900*	+*
						99%	0.95*	2700*	+*
						98%	0.7756	17.2	-
						95%	0.7552	16.8	-
						90%	0.7134	16.21	-
Case 13	17.846	300.41	356.28	3837	1575627	106%	0.8416	58.52	+
						105%	0.795	19.4	+
						100%	0.679	16.4	-

Table 2: Results

Notes to Table 2

CHF: + …increase of T_W and global maximum of (T_W-T_{sat}) at the end of the heated section

    + -…increase of T_W but only local maximum of (T_W-T_{sat}) at the end of the heated section

    - … no increase of T_W at the end of the heated section

q_{calc} / q_{CHF} … ratio of heat flux used in calculating the wall heat flux in the experiment

For example, q_{calc} / q_{CHF} = 90% means that the heat fluxes used in the calculation were:

central rod: $0.9 \cdot q_{CHF}$
middle rod: $0.9 \cdot 0.85 \cdot q_{CHF}$
outer rod: $0.9 \cdot 0.7 \cdot q_{CHF}$ (see distribution of heat fluxes in Fig. 1)

T_w – wall temperature, T_{sat} – saturation temperature, T_{in} - inlet temperature
α_{max} … maximum void fraction in the domain
p_{in} - inlet pressure, mf - mass flux, q_{CHF} - critical heat flux on the central rod

* …not converged solution, calculation crashed

6.1 Typical Results – Case 4, 100% Wall Heat Fluxes

The qualitative results of other cases are similar to the Case 4 results.

Note: For visualization in the following figures, the computational domain is vertically "shrunk" (1:50).
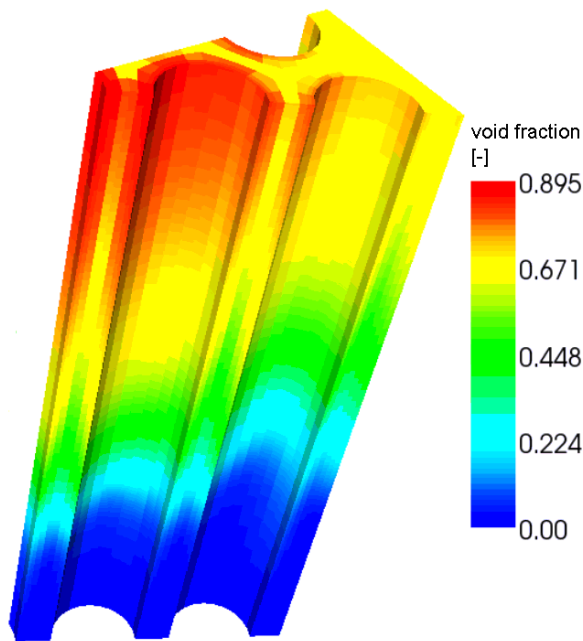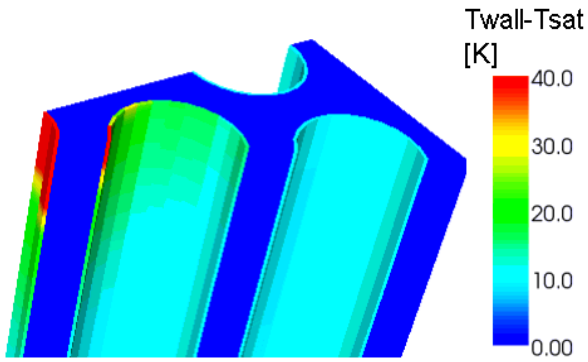

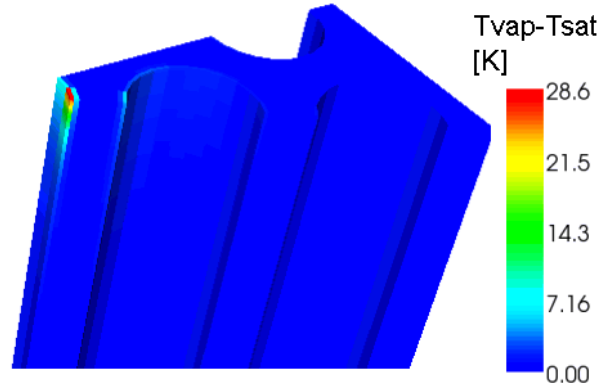**Fig. 4   Case 4, 100% wall heat fluxes: Void fraction [-]**
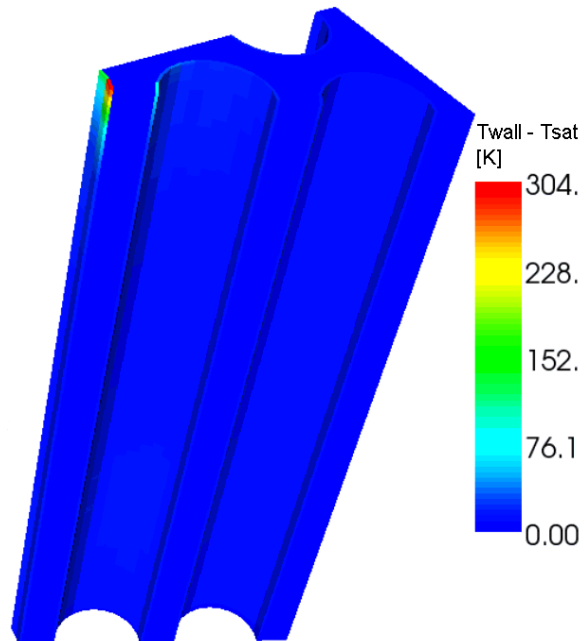
Fig. 5   Case 4, 100% wall heat fluxes: Difference between wall and saturation temperature [K]

Note: the range was clipped to interval <0, max>, zero means that $T_{wall} \leq T_{sat}$
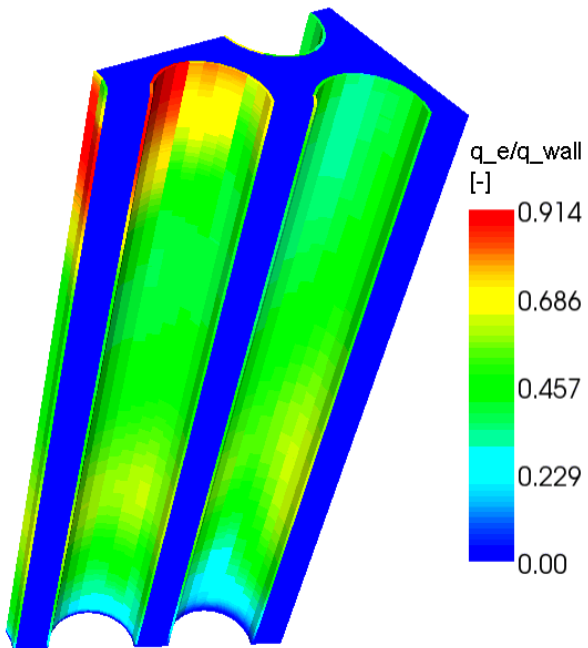
Fig. 6   Case 4, 100% wall heat fluxes: Difference between wall and saturation temperature [K]
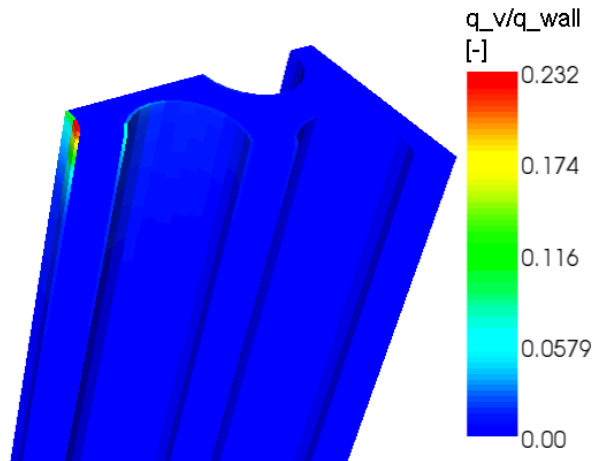
The range was clipped to interval < 0, 40 > K

Fig. 7   Case 4, 100% wall heat fluxes: Difference between vapor temperature and saturation temperature [K]
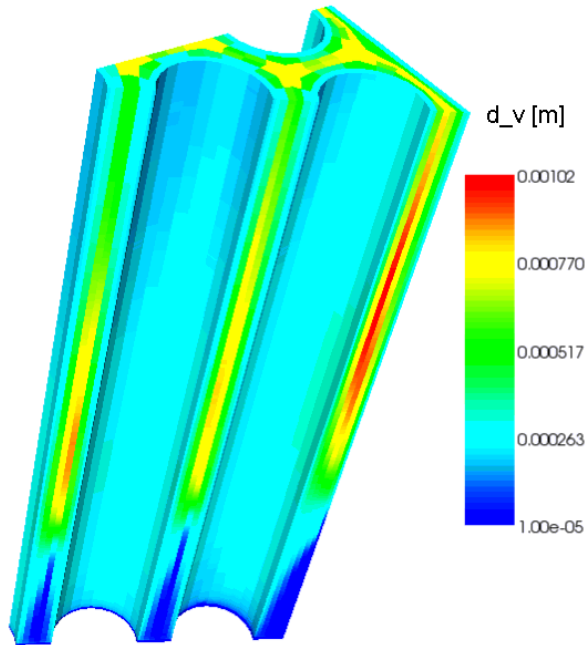
The vapour is heated above the saturation temperature.
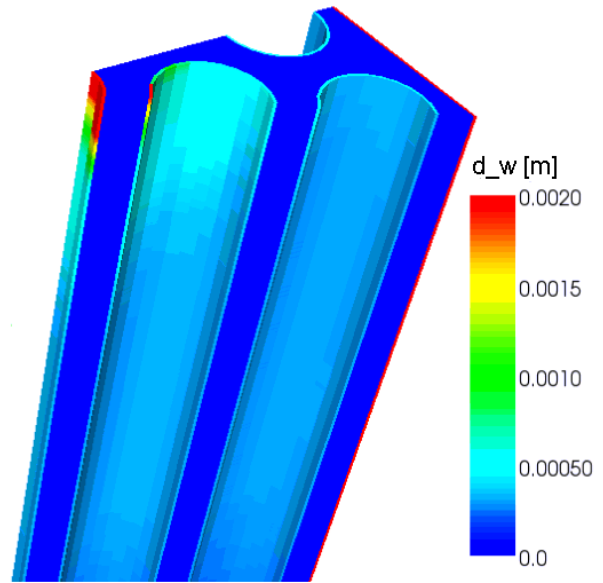

Fig. 8   Case 4, 100% wall heat fluxes: Ratio of evaporation heat flux to total wall heat flux [-]

Fig. 9   Case 4, 100% wall heat fluxes: Ratio of heat flux used for superheating the vapour to the total wall heat flux [-]

Fig. 10 Case 4, 100% wall heat fluxes: Mean bubble diameter [m]

Fig. 11 Case 4, 100% wall heat fluxes: Bubble departure diameter [m]

The bubble departure diameter reached the 0.002m limit set in NEPTUNE.

7. CONCLUSIONS

The capability of NEPTUNE_CFD code to simulate boiling flow with the critical heat flux in a bundle of heated vertical rods has been assessed. 13 Large Water Loop CHF tests have been simulated. In these simulations, a generalized wall heat flux partitioning model that enabled the vapour to be superheated was used.

In all the calculated tests, a sudden rise of the wall temperature at the end of the channel was observed. Simulations of cases with higher mass flux were successful. In these cases, the wall heat fluxes that caused a sudden rise of the wall temperature were in the range of 80 to 110% of experimental heat fluxes. When a sudden increase of the wall temperature occurred, the calculated void fraction at the end of the heated section was higher than 0.8. (Weisman DNB criterion is void fraction = 0.82).

In one case with a low mass flux (Case 3), the region with a sudden rise of wall temperature occurred with 60% of experimental wall heat fluxes. In another case with a low mass flux (Case 11), when the wall heat fluxes were set to 75% of the experimental values, the maximum void fraction at the end of the heated section was 0.84. This indicates that the modelling approach might not be suitable for lower mass fluxes.

The results show that NEPTUNE has some potential for predicting the boiling flow up to CHF in the geometry of reactor fuel assembly.

REFERENCES

Bestion, D., Caraghiaur, D., Anglart, H., Péturaud, P., Krepper, E., Prasser, H M., Lucas, D., Andreani M., Smith B., Mazzini D., Moretti F., Macek J.: "Deliverable D2.2.1: Review of the Existing Data Basis for the Validation of Models for CHF". *NURESIM-SP2 Deliverable* (2006)

Hsu, Y.Y.: "On The Size Range Of Active Nucleation Cavities On A Heating Surface", *J. Heat Transfer 84*, pp.207-216, 1962

Ishii, M., Zuber, N.: "Drag coefficient and relative velocity in bubbly, droplet or particulate flows", *AIChE Journal Vol.25, No.5*, pp. 843-855 (1979)

Kurul, N., Podowski, M.Z.: "Multidimensional Effects in Forced Convection Subcooled Boiling", *Proceedings of the 9th International Heat Transfer Conference*, Jerusalem, Israel, 21-26 August (1990)

Lance M., Lopez de Bertodano M.: "Phase distribution phenomena and wall effects in bubbly two-phase flows", *Multiphase Science and Technology* 8, pp. 69-123 (1994)

Lavieville, J., Quemerais, E., Boucker, M., Maas, L.: "NEPTUNE CFD V1.0 User Guide (Draft)", EDF (2005a)

Lavieville, J., Quemerais, E., Mimouni, S., Boucker, M., Mechitoua, N.: "NEPTUNE CFD V1.0 Theory Manual", EDF (2005b)

Morel Ch., Yao W., Bestion D.: "Three dimensional modelling of boiling flow for the NEPTUNE code", *NURETH-10*, Seoul, Korea, Oct.5-9 (2003)

Ünal, H.C.: "Maximum bubble diameter, maximum bubble growth time and bubble growth rate during subcooled nucleate flow boiling of water up to 17.7MW/m^2", *Int. J. Heat Mass Transfer 19*, pp.643-649, (1976)

Weisman J., Pei B.S.: "Prediction of Critical Heat Flux in Flow Boiling at Low Qualities", *Int. J. Heat Mass Transfer 26*, pp. 1463-1477 (1983)

Yao W., Morel C.: "Volumetric interfacial area prediction in upward bubbly two-phase flow", *Int. J. Heat and Mass Transfer* 47, pp. 307-328 (2004)

Yao W., Morel C.: "Prediction of parameters distribution of upward boiling two-phase flow with two-fluid models", *ICONE10-22463*, Arlington, VA, April 14-18 (2002)

Zuber, N.: "On the dispersed two-phase flow in the laminar flow regime", *Chemical Engineering Science 19*, pp 897. (1964)